Query Details Back to Main Page

1. **Please confirm the corresponding affiliation is correctly identified and amend if necessary.**

Correct

Modelling Particle Transport and Deposition in the Human Healthy and Stented Tracheobronchial Airways

M. Malvè, [1,2,3]✉

Email mauro.malve@unavarra.es

C. Sánchez-Matás, [4]

J. L. López-Villalobos, [4]

[1] Departamento de Ingeniería, Universidad Pública de Navarra, Campus Arrosadía s/n, E-31006 Pamplona, Spain

[2] CIBER-BBN, Centro de Investigación Biomédica en Red - Bioingeniería, Biomateriales y Nanomedicina, C/Poeta Mariano Esquillor s/n, 50018 Zaragoza, Spain

[3] Aragón Institute of Engineering Research, Universidad de Zaragoza, C/María de Luna s/n, 50018 Zaragoza, Spain

[4] Department of Thoracic Surgery, University Hospital Virgen del Rocío, Avenida Manuel Siurot s/n, 41013 Sevilla, Spain

Received: 18 November 2019 / Accepted: 15 March 2020

Abstract

The main goal of this study is the quantification of the particle transport and deposition within the human airways during light, normal and exercise breathing conditions *using the computational fluid dynamics*. In particular we presented a comparison between healthy and stented airways. The considered tracheobronchial model is based on the Weibel symmetric model in which we have inserted the Dumon prosthesis at different locations and on the CT-based geometries of a healthy and a stented airway. The results indicate an important redistribution of the particle deposition locations. Local overdoses can be found in the proximal regions of the prostheses, independently of the breathing conditions, of the particle size and of the considered geometry. The presented work is aimed to contribute to the understanding of the particle deposition in the human lung and to improve drug-aerosol therapies. For patients that underwent airways reconstructive surgery, it can give detailed information about the deposition efficiency and it may help targeting specific airways regions.

Keywords

Particle deposition
Computerized tomography
Computational fluid dynamics
Tracheobronchial airways
Endoprosthesis
Breathing conditions

Associate Editor Ender A. Finol oversaw the review of this article.

Introduction

Aerosol drug therapy mainly consists in delivering the drug in the human respiratory system. Drug inhaled through the mouth should theoretically reach specific regions within the tracheobronchial tree such as large and/or small airways conducts. Unfortunately, even though inhalers devices are designed for delivering the aerosol particles maximizing their deposition, the latter takes place in variable regions of the respiratory tract, mainly in the upper airways.14 This non-optimal distribution finally results in undesirable and dangerous side

effects for the patient apart of a non-useful depositions and a drug waste. It is known that the transport, the magnitude and the location of particle deposition within the human airways depend on the aerosol particle size and the breathing flow rate.14,20,24 Since detailed information within bifurcating airways is difficult to be obtained experimentally, in recent years, the computational fluid dynamics (CFD) has been used for analysing and providing such knowledge as a function of variable breathing conditions. A wide range of micro and nano particles has been numerically simulated in symmetric and asymmetric idealized trees for computing particle trajectories. Straight tubes based on the human airways anatomy has been used for evaluating particle transport and deposition by Refs. 3, 4, 16, 28 and 29. Nevertheless, other works have studied patient specific geometries of human lung including a variable number of tracheobronchial tree generations.12,19,20,23,24 Recent advanced in this field have been focused on the comparison between idealized and realistic or patient specific data of the human airways.22,23 These studies have shown substantial differences between a realistic geometry and a simplified one concluding that the particle deposition and transport is more accurately predicted by realistic geometries. In spite of these findings, idealized Weibel models27 are still used for giving a first insight or some qualitative results on particle transport and depositions.4–6 Despite the knowledge on the computation of particle transport and deposition acquired for healthy subjects, less interest has been given to the deposition of particles in case of obstruction that have been analyzed only in few studies.10,17,30 Chen *et al*.2–4 provide a comprehensive study in this sense, using a Weibel-based model. However, the mechanism of lung injury due the to particles inhalation and deposition is still the object of the study. Hence, a detailed analysis of micro particle transport phenomena in the human airways is needed for a better understanding of the fluid-particle dynamics, and for providing more useful information for health risk assessment and/or drug aerosol therapy improvements. This is especially important for patients with pulmonary diseased and patient that underwent surgical reconstruction or intervention of the airways. Chronic obstructive pulmonary disease (COPD) incidence is estimated around 10% in adult patients.1 Chronic bronchitis and emphysema are the main affections although there are many diseases that lead to airway obstruction. They all promote increased airflow resistance due to airway inflammation, edema and mucus retention.

AQ1

The airways stents solve the acute obstruction but they modify the inner lumen of the airway and hence the airflow.17 However, they have several

contraindications. The implantation of a device promotes inflammations and tissue reactions among others negative effects.8 Therefore, it is clear that local concentration of particles inhaled from the atmosphere or local overdoses of aerosol or other drugs may enhance these situations and further knowledge is necessary for improving eventual therapies and the overall clinical outcomes. As far as the authors know, although in the literature there are a few studies that report particle depositions in case of constricted or obstructed airways,2,10,30 the potential benefits of inhaled therapy in patients with airway stents has not been studied.

The present work is oriented to the characterization of the particle transport and deposition of healthy idealized and CT-based respiratory tract in comparison with stented airways. The idealized models allow analyzing different situations (or different stents) while patient specific models provide more precise depositions in real configurations. A systematic analysis is presented with the aim of providing a detailed understanding of particle regional distribution in the airways of patients that underwent surgical prosthesis implantation.

Materials and Methods

Geometry: Idealized airways model

The particle deposition was studied in a double bifurcating model with generations GEN0-GEN1 and GEN0-GEN2 respectively.16 Its dimensions are similar to those of Weibel symmetric model27 with a branching angle 60° for each bifurcation. In particular, the diameters of the generation 0, 1 and 2 are 1.8, 1.2 and 0.8 cm respectively while the corresponding length are 12, 4.5 and 1.9 cm. For sake of simplicity, the effects of out-of-plane bifurcations have not been considered in the present analysis.4, 5,28 The idealized airways model has been created by means of the commercial package Rhinoceros© (Robert McNeel and Associates, Seattle, WA, USA) and consisted of a series of straight vessel tubes. The model includes the trachea down to the GEN2 and it is represented in Fig. 1a along with a zonal subdivision of the geometry. Finally, the inlet and outlet regions have been sufficiently extended for *damping* the effect of the imposition of the boundary conditions such as plugged inflow and backflow effects.26 After a sensitivity analysis performed on the healthy Weibel-based model, we found that a length of 5 diameters is sufficient for this scope. The extensions allow fully developed flow on the idealized model. However, the flow is not necessarily fully developed in the reality due to the presence of the nasal regions, the larynx and other geometrical changes

affecting the trachea and the asymmetric bifurcations. As the Weibel model is idealized and it is made of a repetitive successions of perfect tubes, the flow can actually develop, at least in the trachea. In this sense, and for comparison purpose within Weibel-based models, the fully developed flow as boundary conditions for their analysis can be justified.

Figure 1

Idealized Weibel-based (a) and patient specific airways geometries (b) healthy and (c) stented respectively) with close-up view to the grid resolutions at the inlet and at the bifurcation. The used Dumon stents are included beside each model. The zonal division in both cases is represented by different colors.

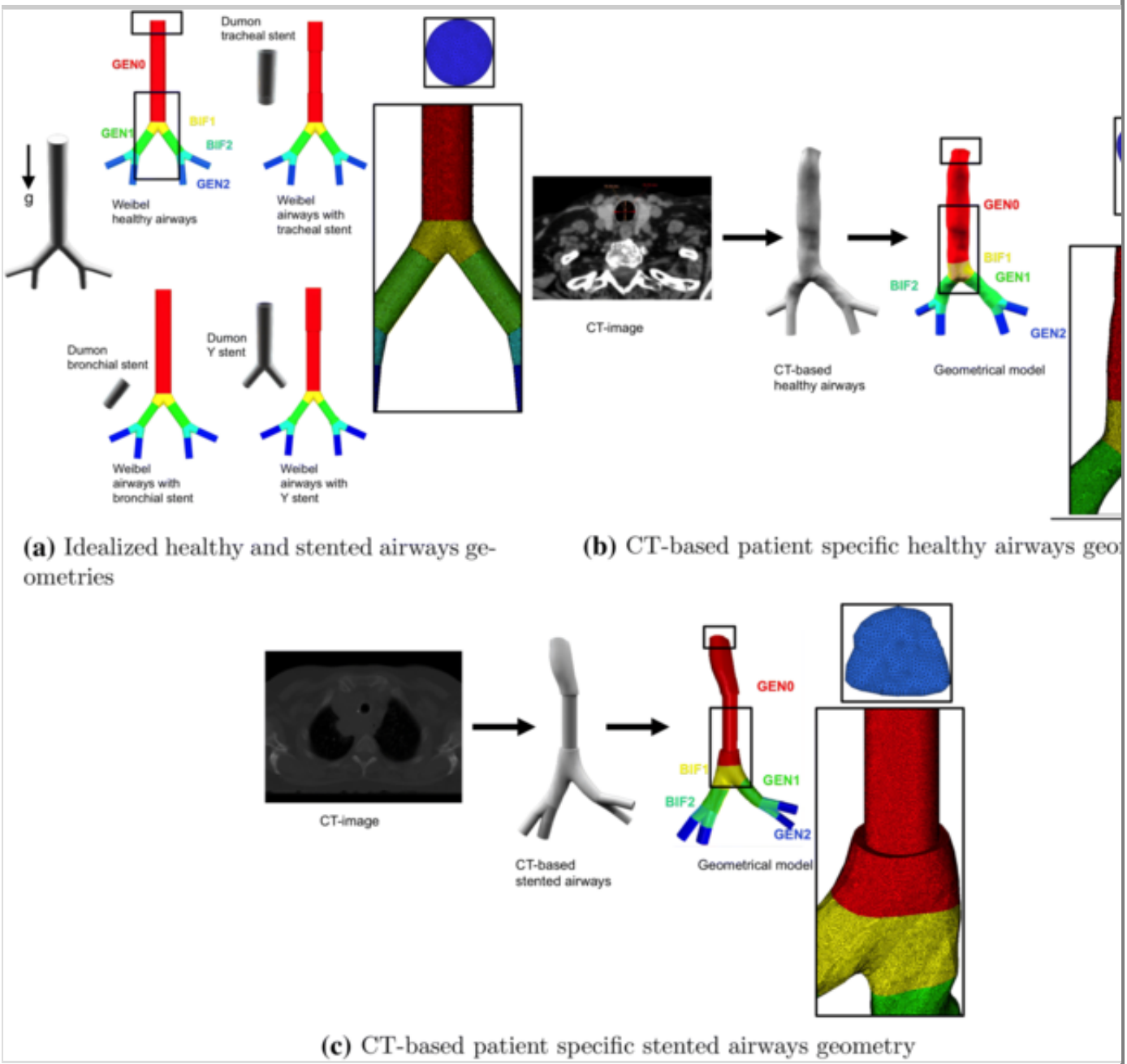

(a) Idealized healthy and stented airways geometries

(b) CT-based patient specific healthy airways geo

(c) CT-based patient specific stented airways geometry

Figure 2

Comparison between the velocity streamlines of the healthy and stented airways at steady inhalation (30 L/min). In each case, axial velocity contours depicted on selected airways cross sections are shown.

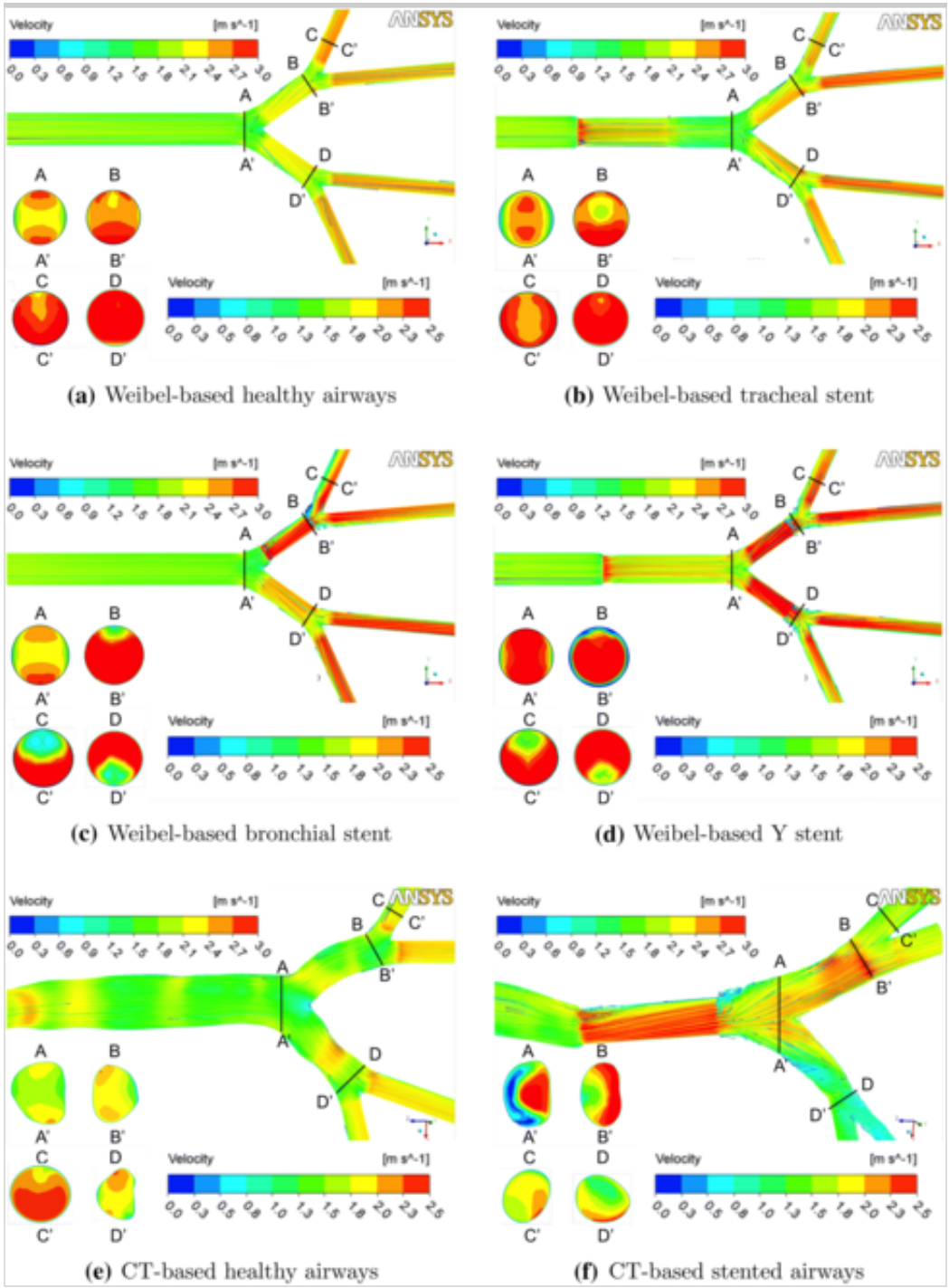

(a) Weibel-based healthy airways

(b) Weibel-based tracheal stent

(c) Weibel-based bronchial stent

(d) Weibel-based Y stent

(e) CT-based healthy airways

(f) CT-based stented airways

Using the Weibel-based geometry, three different prostheses have been inserted in the trachea, in one of the main bronchi and in the carina. In particular we have considered the Dumon stent, i.e. a tracheal, a bronchial and a carina Y prosthesis (see Fig. 1a). In the Table 1 the main geometrical features of the stents are described.

Table 1

Table 1

Main dimensions of the considered silicone Dumon endoprostheses.8

	Thickness [mm]	**Length [mm]**	**Inner diameter [mm]**
Tracheal stent	1	40	16
Bronchial stent	1	30	10
Y stent	1	40/30/30	15/10/10

The three dimensions given for the Y stent refer to the three segments of the device Why this sentence is placed at the boom of the Table? Please note that it is a part of the Table caption and shoul be placed at the top:

Table 1
Main dimensions of the considered silicone Dumon endoprostheses[8]. The three dimensions given for the Y stent refer to the three segments of the device.

Figure 3

Comparison of the computational results of the present Weibel- and CT-based model with the *numerical* findings of Nowak *et al.*19 (a) and with the predictions of the *in vitro* model of Martonen *et al.*18 (b). The comparison was performed using laminar and turbulent flow rate of 28.3 L/min and 45 L/min respectively along the generations GEN 0, GEN 1 and GEN 2 of the model depicted in Fig. 1.

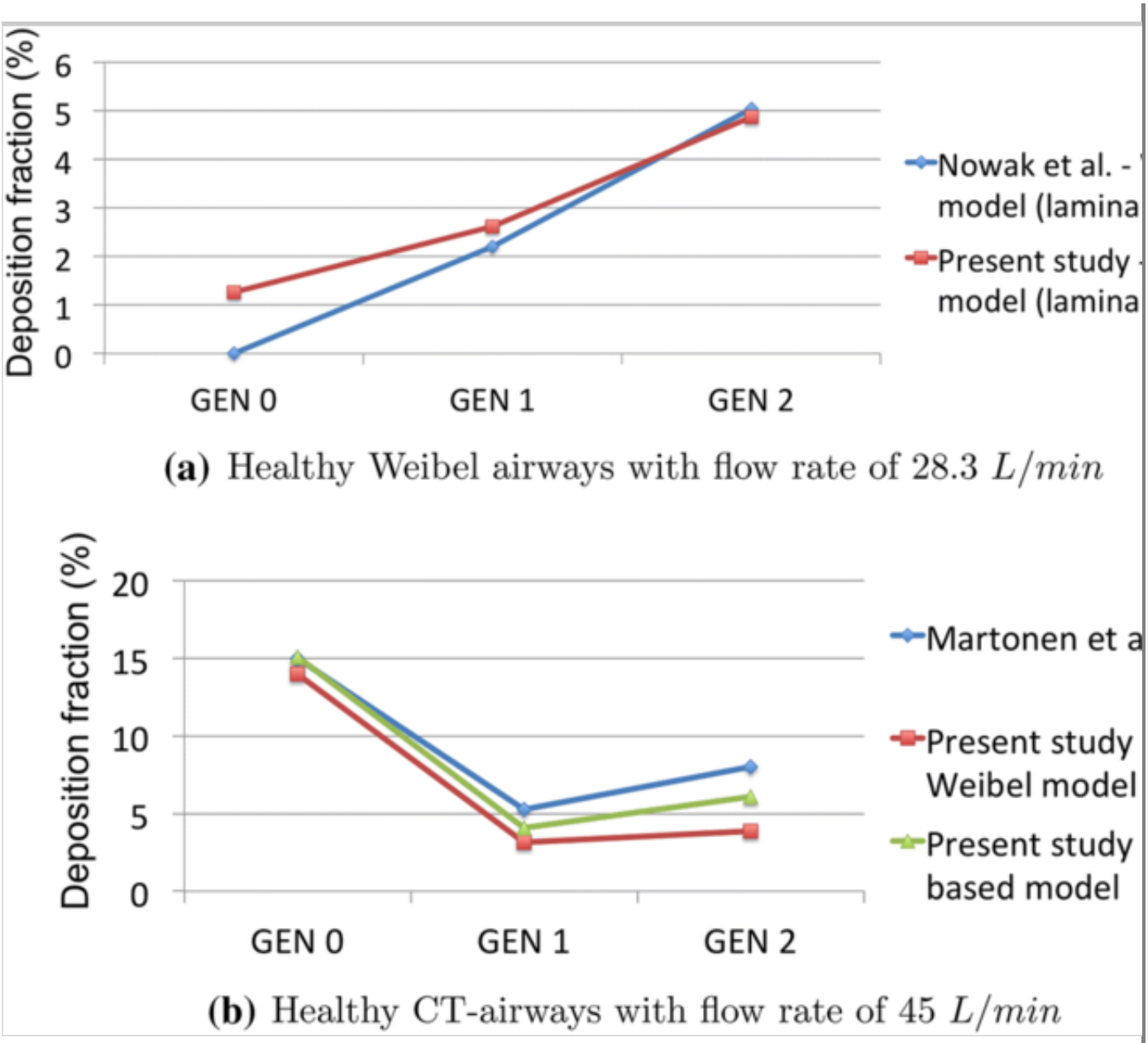

Geometry: CT-Based Model

While the Weibel model allows introducing different types of prosthesis, the patient specific models require additional work related to the images segmentation but they provide more precise information.23 The patient specific geometries were extracted from computerized tomography (CT) images of two healthy adult subjects, one healthy and one in the presence of a Dumon tracheal prosthesis. The DICOM files were imported in the commercial software package MIMICS© (Materialise, Leuven, Belgium). A semi-automatic segmentation was carried out in order to generate the three-dimensional models that were exported as stereolithography (STL) file. Finally, the Weibel-based and the CT-based healthy model were used at selected flow conditions for validating the overall methodology. In particular, a comparison with numerical ~~and experimental~~ literature data was carried out.18,19

Figure 4

3D histograms of the deposition fraction of different zones for two particle diameters ($d_{\{p\}}$) and two different breathing conditions along the healthy and the stented geometries: (a) $d_{\{p\}} = 10\ \mu$m, flow rate = 15 L/min, (b) $d_{\{p\}} = 5\ \mu$m, flow rate = 15 L/min, (c) $d_{\{p\}} = 10\ \mu$m, flow rate = 30 L/min and (d) $d_{\{p\}} = 5\ \mu$m, flow rate = 30 L/min.

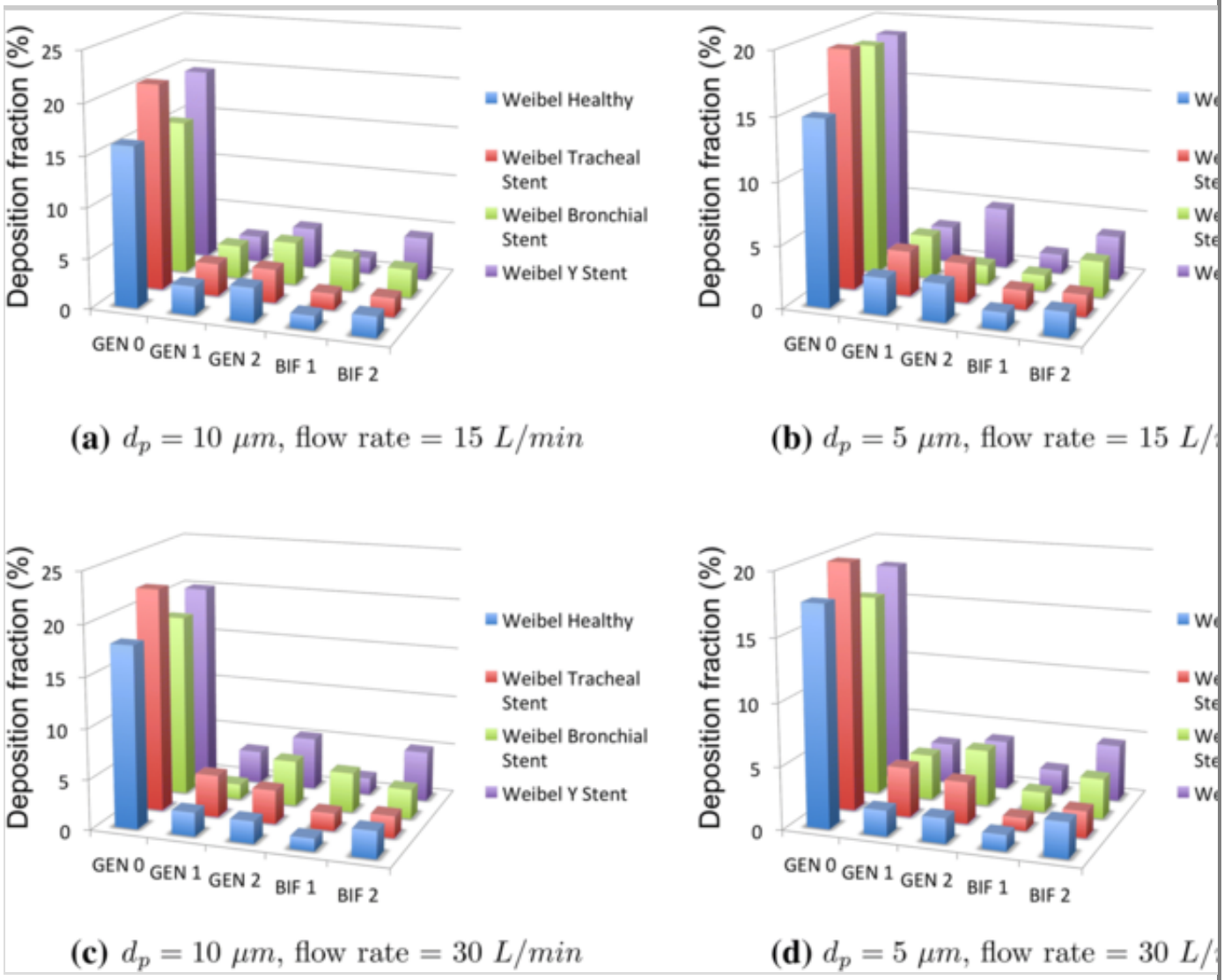

Figure 5

3D histograms representing the regional deposition fractions for particle diameter of 15, 10, 5 and 2 μm and inspiratory flow rate of 15, 30 and 60 L/min.

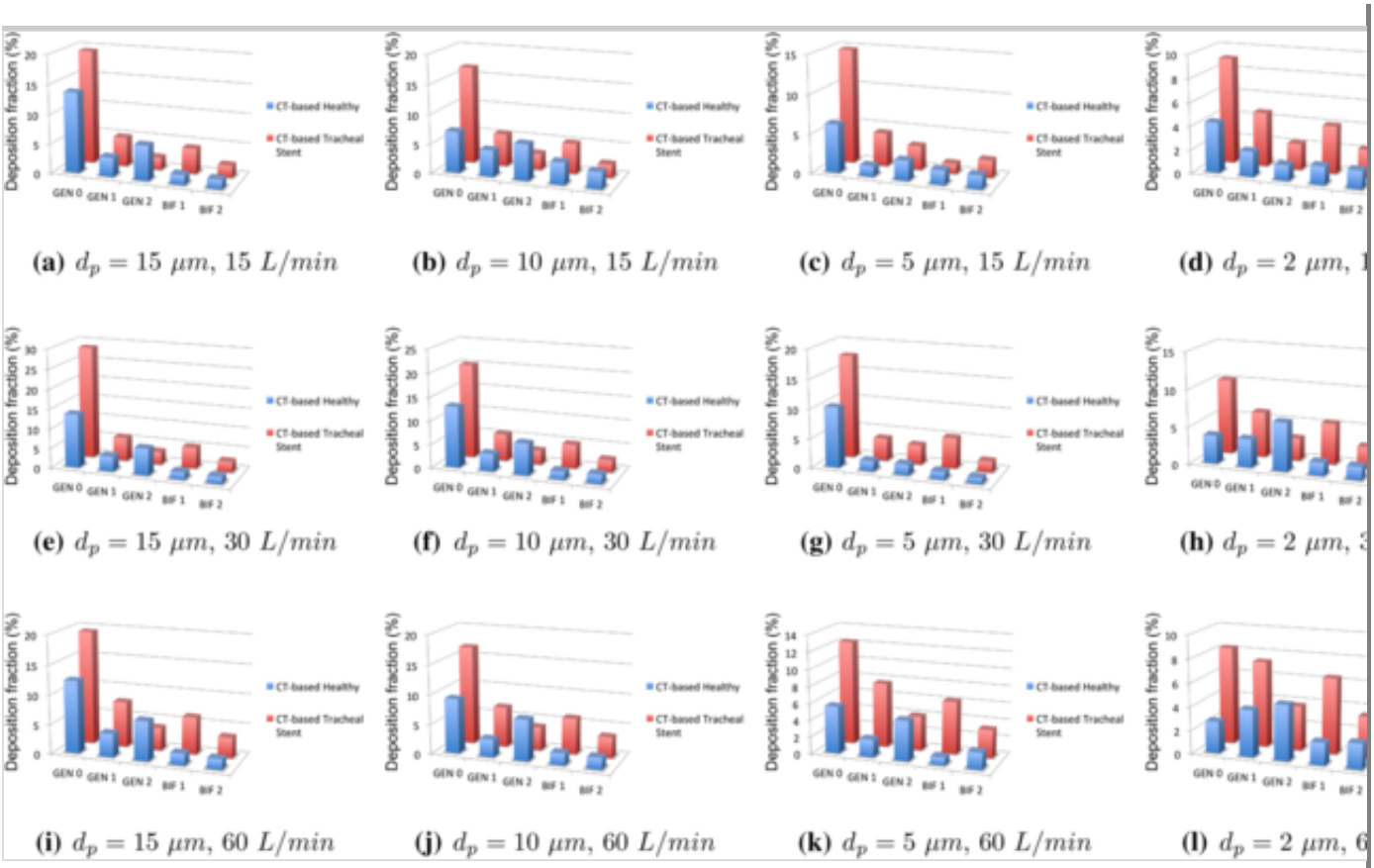

(a) $d_p = 15\ \mu m$, $15\ L/min$ (b) $d_p = 10\ \mu m$, $15\ L/min$ (c) $d_p = 5\ \mu m$, $15\ L/min$ (d) $d_p = 2\ \mu m$, 1

(e) $d_p = 15\ \mu m$, $30\ L/min$ (f) $d_p = 10\ \mu m$, $30\ L/min$ (g) $d_p = 5\ \mu m$, $30\ L/min$ (h) $d_p = 2\ \mu m$, 3

(i) $d_p = 15\ \mu m$, $60\ L/min$ (j) $d_p = 10\ \mu m$, $60\ L/min$ (k) $d_p = 5\ \mu m$, $60\ L/min$ (l) $d_p = 2\ \mu m$, 6

Numerical Modeling and Boundary Conditions

Unstructured tetrahedral computational grids were generated using the commercial software Ansys ICEM CFD, Version 16.0 (ANSYS Inc., Canonsburg, Pennsylvania). To ensure independent results from the mesh element size, a mesh independency study was carried out. In particular, we considered as converged a mesh providing velocity profiles within 5% from the finest tested mesh.4 We tested four different grids of 0.75 millions, 1.5 millions, 3 millions and 6 millions elements. Convergence was reached with the grid size of 1.5 millions elements (see Fig. 1). To fully capture the turbulent boundary layer profile at the near wall regions, the mesh structure includes 5 prism layers at the geometry surface. Considering the turbulence model used in this study, the y^+ value for the mesh refinement used was less than 1. This value is sufficiently small for resolving the near-wall turbulent fluid dynamics.24 Steady conditions are assumed for the airflow.12,15,23,24 CFD simulations were carried out using the commercial software Ansys Fluent, Version 16.0 (Ansys Inc., Canonsburg, Pennsylvania). This software is well known in the scientific community for solving such problems and details of the software methodology, algorithms and other information are given in the Ansys documentation. The solution of the flow field was assumed as converged when the scaled residuals decreased to less than 10^{-6}. This criterion is a standard limit in the literature of

the field of the analysis of particle deposition and transport in human upper airways.21–24,30 The material (air) was assumed to be an incompressible and Newtonian fluid ($\rho = 1.225$ kg/m^3, $\mu = 1.83 \cdot 10^{-5}$ kg/(m $\cdot$ s)). The airways walls were assumed to be rigid with a no-slip boundary condition. Constant flow rates of 15 L/min, 30 L/min and 60 L/min that corresponds to light, normal and heavy breathing conditions respectively,18,24,28 were imposed at the inlet of the CT-models. For the Weibel models, that are simulated as a proof of concept, constant flow rates of 15 L/min, 30 L/min are adopted. At each outlet a 0 *Pa* pressure condition24 was imposed. The used mass flow rates and the corresponding inlet velocities are summarized in the Table 2. For validation purpose, the healthy Weibel-based model was simulated with a laminar flow rate of 28.3 L/min that was used by Nowak *et al*.20 and with a turbulent flow rate of 45 L/min that were used by Martonen *et al*.18 For the pressure-velocity coupling, we used the SIMPLEC algorithm offered by Ansys Fluent. The different terms of the transport equations were discretized using the second-order upwind numerical scheme. As turbulent model, the $k - \omega$ SST model was used.14,23,24,28

Table 2

Characteristics of different breathing conditions.

	Light breathing	**Normal breathing**	**Heavy breathing**
Flow rate [L/min]	15	30	60
Inlet velocity [m/s]	0.9825	1.965	3.93

Figure 6

Total deposition fraction for different flow rates and different particle diameters along the Weibel-based and the CT-based healthy and stented airways.

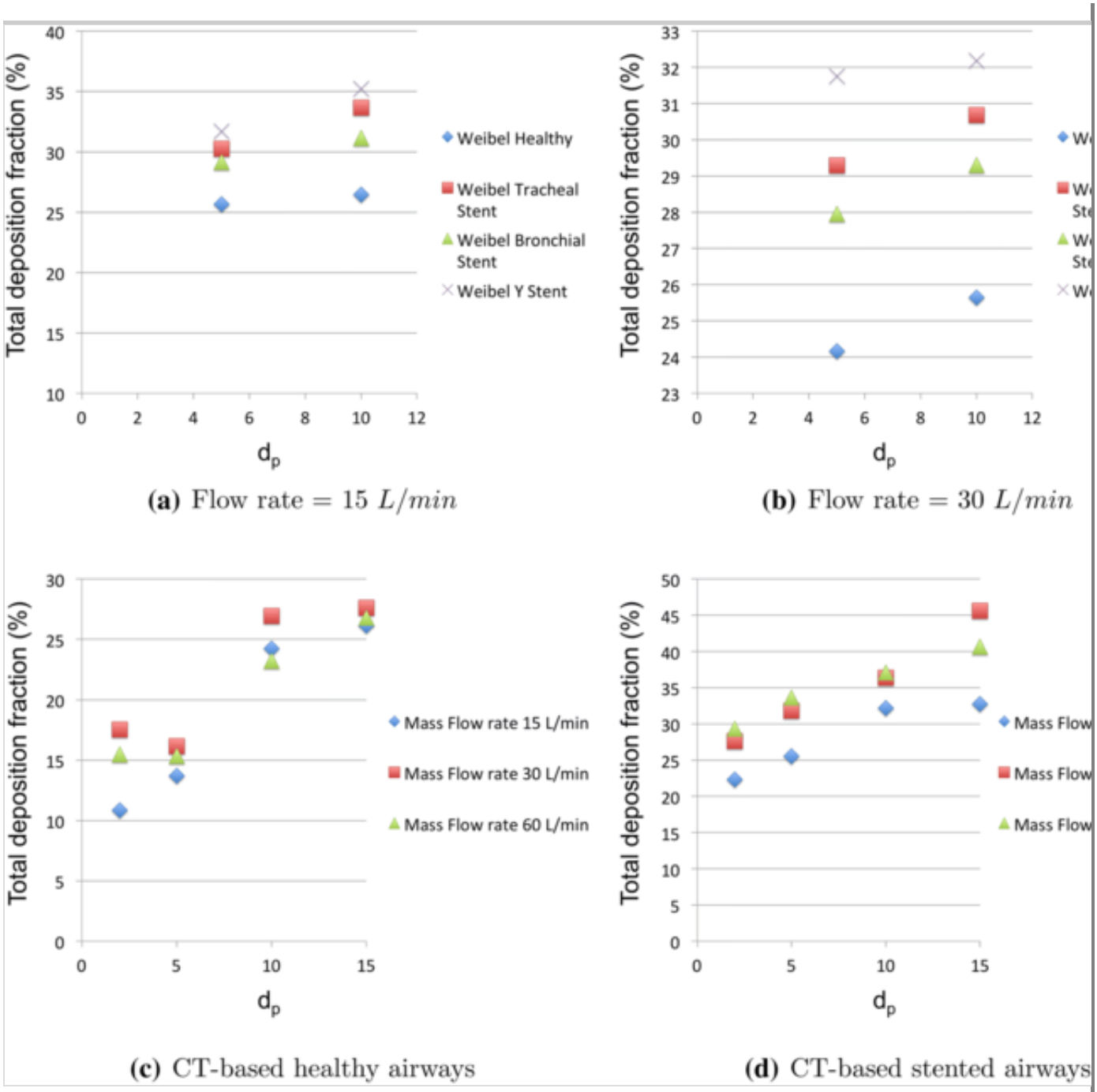

Figure 7

Variation of the deposition patterns (in [μg/cm^2 s]) for different particle sizes at light breathing conditions (15 L/min).

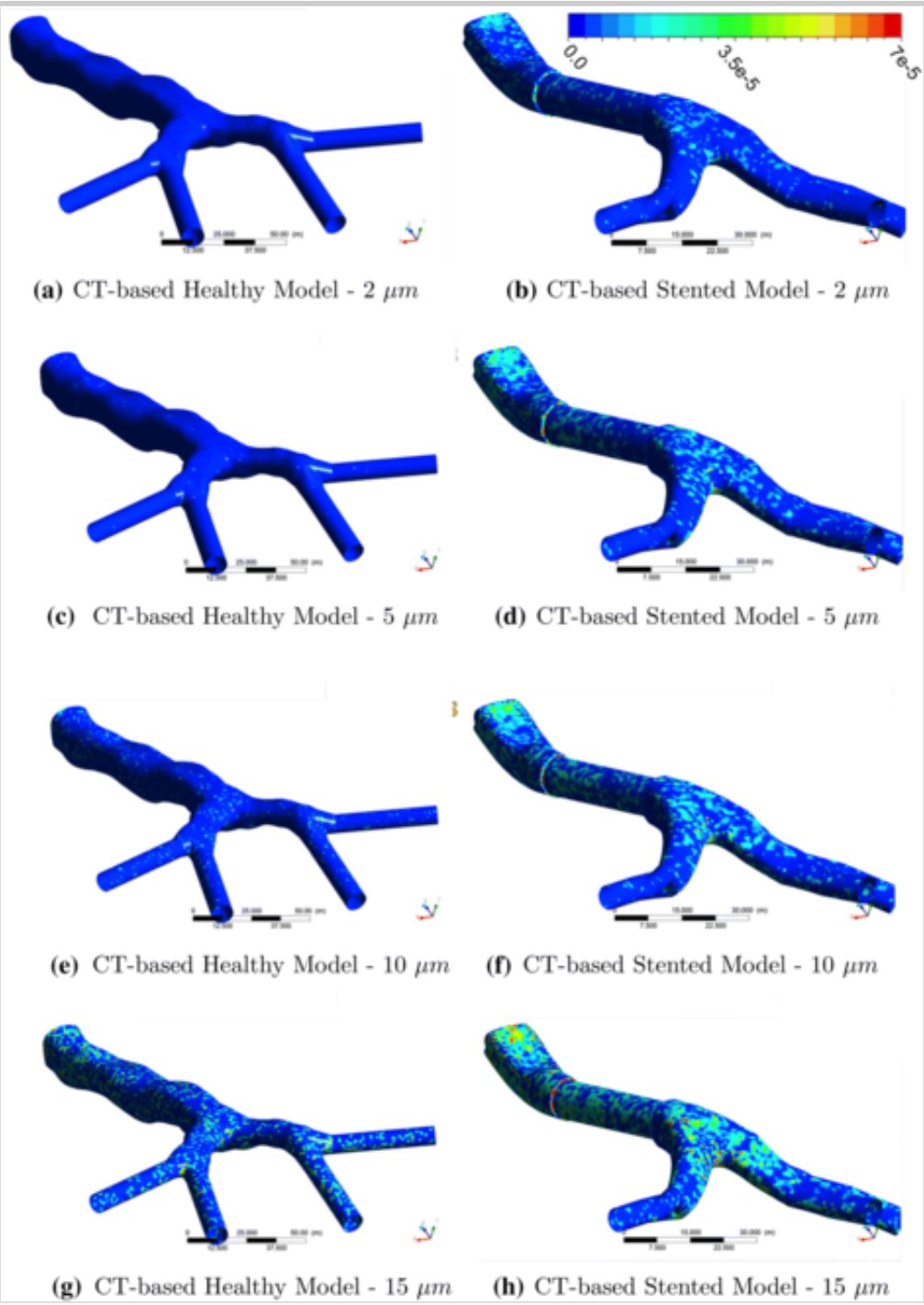

Figure 8

Variation of the deposition patterns (in [μg/cm^2 s]) for a fixed particle diameter of 10 μm as a function of different inspiratory flow rate of 15 L/min (a), 30 L/min (b) and 60 L/min (c).

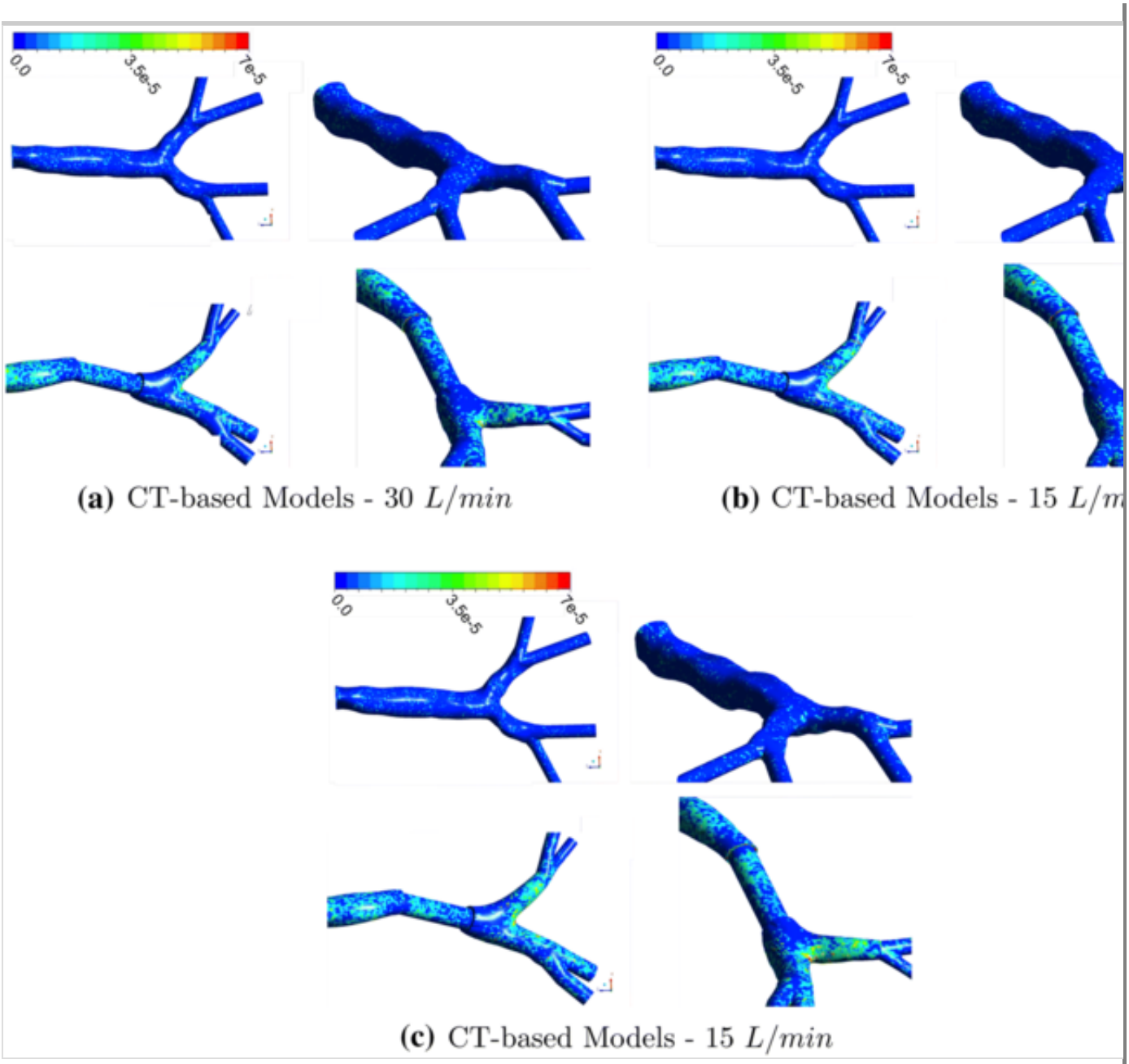

(a) CT-based Models - 30 L/min

(b) CT-based Models - 15 L/m

(c) CT-based Models - 15 L/min

Discrete Phase Modeling

The commercial software Ansys Fluent offers several applications using the discrete phase model (DPM) as the aerosol transport and deposition considered in this study. The particle tracking is performed in a Lagrangian reference frame that is applicable for a low volume fraction of the dispersed particle phase. In this reference, each particle are individually followed defining its initial position, velocity, size and temperature. The computation of the trajectories is based on a force balance, using the local continuous phase conditions as the particle moves through the flow. This is performed integrating the force balance that can be expressed as follows:

$$\sum F = m_{\{p\}} \frac{\{d\}u_{\{p\}}}{\{d\}t}$$

where $u_{\{p\}}$ is the particle velocity and F is the force term which includes several terms. However, due to the small value of particle Reynolds number ($<< 1$), the large value of fluid-particle density ratio ($\rho/\rho_{\{p\}} >> 1$) and the size of the considered particles, most of this terms can be neglected.22 In the present study, we used only the contribution of the drag and of the gravitational force.

The equation describing the particle velocity, in the Lagrange formulation, for a Cartesian coordinate system can be written in the form:

$$\frac{\partial u_p}{\partial t} = F_D(u - u_p) + \frac{g(\rho_p - \rho)}{\rho_p}, \quad 2$$

where u is the fluid velocity, $d_{\{p\}}$ is the particle diameter. The term $F_D(u - u_p)$ is the drag force per unit particle mass and F_D can be computed as:

$$F_D = \frac{18\mu}{\rho_{\{p\}} {d_{\{p\}}}^2} \frac{c_{\{D\}} Re_{\{r\}}}{24}, \quad 3$$

where c_D is the drag coefficient, μ is the dynamic viscosity of the fluid and $Re_{\{r\}}$ is the particle Reynolds number that involves its relative velocity with the fluid. The drag coefficient and the relative Reynolds number are computed as follows:

$$c_D = \frac{k_1}{Re_{\{r\}}} + \frac{k_2}{{Re_{\{r\}}}^2} + k_3, Re_{\{r\}} = \frac{\rho d_{\{p\}}(u_{\{p\}} - u)}{\mu}, \quad 4$$

where k_i, $(i = 1, 2, 3)$ are constants.23,24

Particles of specific sizes were injected in a uniform distribution at the inlet face of the computation domain, and tracked through the geometry until they found one of the three specific conditions: they collide and are trapped on the airways walls, they escape from the domain through one of the outlet faces or they continue suspension in the flow. The present work considers two-way coupling between airflow and particle motion. The latter means that the fluid (continuous phase) and the particles motion (discrete phase) are mutually affected by each other. However, since the particles size is sufficiently small and the suspension is dilute, the effect of the particles on the airflow is actually

negligible. The continuous phase was performed previous to the discrete phase. Particles were considered as spherical, with a density of $\rho_{\{p\}} = 1000$ kg/m^3, a diameter of $d_{\{p\}} = 2, 5, 10, 15\ \mu$m and a velocity equal to that of the model inlet.24 These particular particle diameters have been chosen for simulating the typical micro particle that characterize the aerosol. For ensuring that the results were independent on the number of injected particle, a sensitivity study for the particles was carried out. After the analysis, over 11,000 particles for each size were injected through the inlet of each considered model.

Results

Flow Patterns of the Healthy and Stented Model

Weibel-Based Model

In this section, the main features of the airflow for the healthy and the stented airways are presented for giving an overview of the device influences on the flow patterns. This comparison is qualitatively given for the flow rate 30 L/min but it is valid also for the flow rate 15 L/min. The velocity magnitude, of course increases by increased inspiratory flow rates and secondary flows vortices tend to become larger.

In the Fig. 2, the flow patterns for the healthy airways are shown by means of three-dimensional streamlines and planar contours of velocity magnitude. Comparing the healthy and the stented airways, considerable differences can be seen. In particular, the presence of the device promotes in all the considered cases a variation of the local flow patterns. For the healthy case (Fig. 2a), as expected, at the carina, the flow divides and a secondary velocity field develops into the main bronchi. Secondary flows develop also at the second flow divider. The tracheal device, on the contrary, not only changes the velocity patterns at the trachea but also influences the flow regime downstream, in the lower generations (Fig. 2b). This aspect is also enhanced in the airways model in the presence of the bronchial device (Fig. 2c). While a local acceleration is promoted in the bronchus where the device is located, the flow seems to be altered also in the other bronchus and in the lower generations, compared with the healthy airways. Finally, the Y stent seems to be the most impacting device (Fig. 2d). The flow patterns are in fact altered at the trachea and in both main bronchi, where the device is located. The presence of the device promotes a local acceleration and deceleration of the flow and also a change of the intensity of the secondary flow structures that develop inside the generations GEN1 and

GEN2.

CT-Based Model

The results found in the Weibel based geometries allow extracting qualitatively similar conclusions to what can be found for the CT-models. However, quantitative differences can be seen. In the Fig. 2 (lower panel), it is shown that secondary flows develop into the main bronchi for both healthy and stented geometries. Moreover, the prosthesis markedly impacts the tracheal flow due to the reduction of the lumen promoted by its introduction. The impact is not limited to the first generation but it is also extended to the successive generations after the carina as for the Weibel model. Interestingly, it can be seen an important asymmetric distribution of the flow especially enhanced for the stented model respect to the healthy case (compare Figs. 2e and 2f). This is due to the slightly higher asymmetry of stented geometry respect to the healthy model. Additionally, it is visible that the airflow enters the device skewed, as the asymmetry regards not only the bifurcation but also the tracheal tract. This is visible comparing for example the Weibel-based tracheal stented model with the CT-based geometry in the presence of the device. The flow enters the device with a higher velocity and with a skewed direction as its tracheal axis is not straight. Both aspects are important because they have a massive influence on the particle deposition. Also at the bifurcation, the high asymmetry promotes higher airflow velocity in the primary branches and the flow distribution is very asymmetric. A comparison with the Weibel models (see Figs. 2b and 2f) allows seeing that the asymmetry of the airflow regards also the second bifurcation and promotes considerably different velocity patterns in these regions. The Fig. 2f) shows in fact markedly different flow regimes at the second bifurcation comparing both branches. The latter cannot be found neither in the healthy CT-based model (Fig. 2e) nor in the Weibel stented models of the Figs. 2a–2c. All these geometrical and morphological aspects confirms the importance of considering patient specific models for computing more precisely the airflow and, as a consequence, the particle transport and deposition.

Benchmarking Present Study Results with Literature Data

Regional particle deposition obtained in the current work was compared to the numerical results reported by Nowak *et al*.19 and by Martonen *et al*.18 obtained using the Weibel-based model. Firstly, the Weibel-based healthy model has been compared with that of Nowak *et al*. for a particle size of 10 μm, an inhalation flow rate of 28.3 L/min and a laminar flow (see Fig. 3a). Then, the Weibel-

based model and the CT-based airways have been compared with the model of Martonen *et al*. for a particle size of 10 μm, an inhalation flow rates of 45 L/min and a turbulent flow (see Fig. 3b). The deposition fraction accordingly to Zhang *et al*.28 is computed as:

$$DF(\%) = \frac{\text{Number of deposited particles}}{\text{Number of injected particles}} \times 100 \qquad 5$$

With aim of identifying the regional deposition of particles, the airway geometry was segmented into 7 zones according to Fig. 1a. The local deposition fraction in each zone was calculated and plotted for the present models and the aforementioned literature studies.

The comparison performed on the three main generations (GEN 0, GEN 1 and GEN 2 of Fig. 3a shows a good agreement. The main difference regards the particle trapped in the trachea that are zero in the work of Nowak *et al*.19 while are of about 1.26% in the present work (see Fig. 3a). This difference is probably due to the different grid resolution and to the different number of generations considered in these two works.

In the Fig. 3b, the deposition of 10 μm particle of the turbulent simulations for the Weibel- and CT-based airways models is compared in the aforementioned 3 generations GEN 0, GEN 1 and GEN 2 with the findings of Martonen *et al*.18 From this comparison it appears that the deposition obtained in the present CFD simulations and those obtained by Martonen *et al*. are of the same order. In particular, it seems that the prediction is more accurately provided in the trachea (see Fig. 3b) while in the following generations differences appear. These can be explained considering the different approach used in these studies and the overall different geometrical model. In general, the computational results seem to slightly underestimate the results of Martonen, as the difference of 1% at the first generation tends to increase in second and in the third generation. In particular, as depicted in the Fig. 3b, the Weibel- and CT-based models at the third generation show a deposition of about 4 and 6% respectively while that predicted by Martonen is higher ($\approx$ 8%).

Comparison of the Particle Deposition Between Healthy and Stented Airways

Weibel-Based Model

Table 3

Regional deposition fractions (in %) of the Weibel-based models for a flow rate of 30 L/min.

$d_{\{p\}} = 10\ \mu$m	GEN 0	GEN 1	GEN 2	BIF 1	BIF 2
Weibel healthy	17.98	2.35	2.2	1.24	2.7
Weibel tracheal stent	22.17	4.21	3.37	1.74	2.18
Weibel bronchial stent	18.2	1.51	4.54	3.96	2.94
Weibel Y stent	20.03	3.26	5.24	1.66	5.03
$d_{\{p\}} = 5\ \mu$m	GEN 0	GEN 1	GEN 2	BIF 1	BIF 2
Weibel healthy	17.53	2.04	1.99	1.275	2.84
Weibel tracheal stent	19.8	3.98	3.36	1.01	2.12
Weibel bronchial stent	16.2	3.64	4.52	1.59	3.21
Weibel Y stent	17.93	3.26	3.96	2	4.56

In the Fig. 4, the comparison between the healthy and the three stented airways is shown. The values of the histograms are summarized in the Tables 3 and 4. As expected, due to the inertial impaction, the deposition tends to decrease for decreasing particle diameter.23,24 From the Fig. 4 it is also visible that the region more affected by the deposition in the presented models, independently of the inspiratory flow rate and of the particle diameter, is the trachea. Furthermore, the histograms show that the presence of a prosthesis, that is technically equivalent to a slight airways constriction, considerably increases the particle *deposition in other regions, as the first generation and the carina*. As obvious, the tracheal stent significantly impacts the particle deposition on the first generation i.e. at the trachea. The related histogram depicted in the Fig. 4 highlights that the highest deposition corresponds always to this prosthesis *at the trachea* independently of the breathing regime and of the particle diameter. *Its maximal value* (22.17%) is reached at flow rate 30 L/min with particle diameter $d_{\{p\}} = 10\ \mu$m. As visible, in the first generation an increase of the flow promotes an increase in the deposition fraction. However, this effect is especially enhanced only for the trachea. The latter, independently on the used device, shows deposition fractions in the range of about 16–19% for flow rates of 15 L/min and of about 18–22% for flow rates of 30 L/min. This represents the largest increase in the deposition fraction alongside all the

generations and depends on the device (the smallest for the bronchial stent, the highest for the tracheal stent) respect to the healthy models. The deposition tends to decrease for increasing respiratory flow in the generations 1 and 2 respect to the trachea. However, significant increases in these generations are presented by the stented models respect to the healthy case. The largest increase can be found for the bronchial and the Y-stent, which first generation is constricted by the presence of the prostheses. The increase in this region is of about 2 and 3 times respectively respect to that found in the healthy model for inspiratory flow of 30 L/min. In these generations, the deposition looks slightly more homogeneous among models, independently of the particle diameter, even the presence of the prosthesis tends to promote an increase of the deposition at the first generation for the tracheal stent, at the first bifurcation (about 4%), at the second generation for the bronchial stent (about 4.5%) and at the second generation and second bifurcation for the Y-stent (about 4 and 5% respectively).

Table 4

Regional deposition fractions (in %) of the Weibel-based models for a flow rate of 15 L/min.

$d_{\{p\}} = 10\ \mu$m	GEN 0	GEN 1	GEN 2	BIF 1	BIF 2
Weibel healthy	15.9	2.85	3.42	1.4	2.07
Weibel tracheal stent	20.6	3.25	3.35	1.61	1.875
Weibel bronchial stent	15.54	3.32	4.29	3.3	2.85
Weibel Y stent	19.63	2.61	4.07	1.6	4.28
$d_{\{p\}} = 5\ \mu$m	GEN 0	GEN 1	GEN 2	BIF 1	BIF 2
Weibel healthy	14.82	2.94	3.03	1.37	2
Weibel tracheal stent	19.2	3.61	3.16	1.55	1.77
Weibel bronchial stent	18.7	3.5	1.56	1.27	2.92
Weibel Y stent	18.8	2.9	4.94	1.56	3.56

This tendency slightly reduces for flow rate of 15 L/min but the main tendencies are still valid. In the trachea, the presence of the device has an important influence. Again the stents promote important increases in the second bifurcation. In this generation, an increases of about a factor 2 can be seen between healthy and Y-stent while at the second generation the Y-stent seems to

promote the highest deposition (4.94%). Finally, while at the first bifurcation the deposition seems more homogeneous and the highest deposition is suggested by the bronchial stent at 30 L/min for $d_{\{p\}} = 10\ \mu$m (about 4%), in the second bifurcation, the Y-stent promotes the highest deposition independently on the particle diameter and on the breathing conditions with values that range from about 3.5 to 5%.

CT-Based Model

Table 5

Regional deposition fractions (in %) of the CT-based models for a flow rate of 60 L/min.

$d_{\{p\}} = 15\ \mu$m	GEN 0	GEN 1	GEN 2	BIF 1	BIF 2
CT-based healthy	12.37	3.96	6.74	1.95	1.76
CT-based tracheal stent	19.4	7.73	3.85	6.26	3.45
$d_{\{p\}} = 10\ \mu$m	GEN 0	GEN 1	GEN 2	BIF 1	BIF 2
CT-based healthy	9.27	2.98	6.98	2	2
CT-based tracheal stent	16.76	6.8	3.95	6.06	3.51
$d_{\{p\}} = 5\ \mu$m	GEN 0	GEN 1	GEN 2	BIF 1	BIF 2
CT-based healthy	5.6	2.07	4.76	0.94	1.99
CT-based tracheal stent	12.34	7.65	4.065	6.24	3.32
$d_{\{p\}} = 2\ \mu$m	GEN 0	GEN 1	GEN 2	BIF 1	BIF 2
CT-based healthy	2.7	4	4.72	1.89	2.16
CT-based tracheal stent	8.3	7.33	3.79	6.43	3.47

Table 6

Regional deposition fractions (in %) of the CT-based models for a flow rate of 30 L/min.

$d_{\{p\}} = 15\ \mu$m	GEN 0	GEN 1	GEN 2	BIF 1	BIF 2
CT-based healthy	13.6	3.75	6.72	1.8	1.75
CT-based tracheal stent	28.6	5.95	3.2	5.24	2.63

$d_{\{p\}} = 10\ \mu$m	GEN 0	GEN 1	GEN 2	BIF 1	BIF 2
CT-based healthy	12.98	3.67	6.7	1.68	1.98
CT-based tracheal stent	20.18	5.7	2.92	5.01	2.56
$d_{\{p\}} = 5\ \mu$m	GEN 0	GEN 1	GEN 2	BIF 1	BIF 2
CT-based healthy	10.29	1.725	1.84	1.3	1.01
CT-based tracheal stent	17.72	3.83	3.283	5.15	1.83
$d_{\{p\}} = 2\ \mu$m	GEN 0	GEN 1	GEN 2	BIF 1	BIF 2
CT-based healthy	3.8	3.78	6.5	1.72	1.74
CT-based tracheal stent	10.2	6.12	3	5.5	2.82

Table 7

Regional deposition fractions (in $\%$) of the CT-based models for a flow rate of 15 L/min.

$d_{\{p\}} = 15\ \mu$m	GEN 0	GEN 1	GEN 2	BIF 1	BIF 2
CT-based healthy	13.7	3.23	5.94	1.67	1.6
CT-based tracheal stent	19.42	4.95	2.07	4.27	2.03
$d_{\{p\}} = 10\ \mu$m	GEN 0	GEN 1	GEN 2	BIF 1	BIF 2
CT-based healthy	7	4	6	3.75	2.84
CT-based tracheal stent	16.63	5.5	2.74	5.1	2.21
$d_{\{p\}} = 5\ \mu$m	GEN 0	GEN 1	GEN 2	BIF 1	BIF 2
CT-based healthy	6.24	1.35	2.54	1.84	1.74
CT-based tracheal stent	14.74	4.28	3.07	1.26	2.2
$d_{\{p\}} = 2\ \mu$m	GEN 0	GEN 1	GEN 2	BIF 1	BIF 2
CT-based healthy	4.3	2.14	1.3	1.55	1.55
CT-based tracheal stent	9.08	4.64	2.23	4.05	2.33

In the Fig. 5, the comparison between the healthy and the stented airways is shown for flow rates of 60 L/min (Figs. 5a–5d), 30 L/min (Figs. 5e–5h) and 15 L/min (Figs. 5i–5l). The values of the histograms are summarized in the

Tables 5, 6 and 7. A qualitative comparison with the Weibel models shows that the patient specific geometries suggest an increase of the deposition. This is expected, because the real geometries provide curvatures and tortuosities that the Weibel models cannot offer. Comparing the CT-based models, *an important increase* of particle deposition is visible in the trachea, in the presence of the prosthesis and independently of the breathing conditions and of the particle dimension. Its maximal value is 19.4%, 28.6% and 19.42% for flow rates of 60 L/min, 30 L/min and 15 L/min respectively, with particle diameter $d_{\{p\}} = 15\ \mu$m. This increase is more enhanced at normal breathing conditions (compare Figs. 5e–5h with Figs. 5a–5d and Figs. 5i–5l). However, a decrease of deposition can be clearly seen for small particle sizes. In fact, for $d_{\{p\}} = 2\ \mu$m, the maximal values reduced to 8.3, 10.2 and 9.08% for flow rates of 60 L/min, 30 L/min and 15 L/min respectively. Obviously, the tracheal stent impacts the particle deposition especially at the trachea while its increase in the successive generations looks more limited, as the values are considerably less that 10%. However, the tendency found with the Weibel models are visible also for the CT-based models. Important increments in deposition fractions are reported by the patient specific models at the first bifurcation. There, the tracheal stent provides systematically higher depositions respect to the healthy case. Its maximal values ranges from 4 to over 6% while the maximal deposition for the healthy case is 3.75% (found at light breathing conditions). This tendency can also be found at the first generation, independently of the flow rates and of the particle size. In these regions, the deposition in the presence of the prosthesis is always from 2 to 3 times higher than that of the healthy patient. This ranges from about 4 to 6.43% for the tracheal stent and from about 2 to 4% for the healthy case.

Comparison of the Total Deposition Fractions Within Stented and Unstented Models

The Fig. 6 depicts the total deposition fraction for different flow rates and different particle sizes along the healthy and the stented airways for both Weibel and CT models. As it can be seen in this Figure, the deposition increases for increasing particle diameter, as found by other authors,14,23 because of the increase of impaction. The Figure clearly shows that, within the Weibel models, the highest total deposition is promoted by the Y-stent independently of the flow rate, for particle diameter of 10 μm (35.2 and 32.2%). This means that the device impacts not only the regions near its location but also downstream the lower generations. This stent promotes in fact a high deposition at the second

generation in all the simulated cases (see also Fig. 4). This result is independent of the flow rate and of the particle diameter. For a flow rate of 15 L/min, the total deposition is also the highest for the Y stent for $d_{\{p\}} = 10\ \mu$ (32.2%). However, the tendency for the Weibel models is markedly clear, as the second highest deposition is always promoted by the tracheal stent and the third one by the bronchial stent, independently on the inspiratory flow rate. In general, an increase of the flow tends to increase the relative differences of the total particle depositions between stented models (compare Figs. 6a and 6b).

In the CT-based healthy and stented airways (Figs. 6c and 6d respectively), it is visible a marked increase of deposition promoted by the prosthesis (Figs. 6c and 6d, 45.62% vs. 27.615%) for 30 L/min and particle diameter $d_{\{p\}} = 15\ \mu$m. The increase can be seen for all the flow rates and particle diameters, by comparing healthy and stented models in the Figs. 6c and 6d. The Figure depicts an increase of deposition for increasing particle diameters even for a flow rate of 30 L/min and 15 L/min, the total depositions for particles of $d_{\{p\}} = 2\ \mu$m are slightly higher than that of $d_{\{p\}} = 5\ \mu$m (17.5% vs. 16.5% and 15.4% vs. 15.3%). Nevertheless, in the literature it has been demonstrated in fact that for particle diameters smaller than $5\ \mu$m, the deposition tend to considerably increase.14 Of course, the deposition for particle of $2\ \mu$m is much smaller that that of 10 or $15\ \mu$m diameters, independently of the flow rate.

Spatial Distribution of the Particle Deposition

Deposition patterns, that illustrate the interaction between the particle and the airways and stent wall, can be represented by means of the accretion ratio of the software Ansys Fluent and they give an idea of the locations where the particles tend to deposit and concentrate in dependence on the particle diameter and flow rate. This variable represents the particle mass flow rate divided by the particle impacted face area and it is computed as30:

$$R_{\{\text{accretion}\}} = \sum_{p=1}^{N} \frac{\dot{m}_{\{p\}}}{A_{\{\text{face}\}}} \tag{6}$$

where N is the number of particles, $A_{\{\text{face}\}}$ is the area of the cell face at the wall, and $\dot{m}_{\{p\}}$ is the mass flow rate of the particles. Since the highest deposition fraction has been systematically assessed in the CT-based models respect to the Weibel-based model, which computations have been mainly provided as a proof of concept, the spatial distribution is represented for the CT-

geometries first for a fixed flow rate of 15 L/min as a function of the particle size (Fig. 7) and then for a fixed particle size of 10 μm as a function of the flow rate (Fig. 8).

The Fig. 7 shows the increase of particle deposition due to the presence of the prosthesis confirming the results observed by means of the histograms (Fig. 5). As visible, the stented airways are significantly affected by the turbulent dispersion respect to the healthy airways. A marked deposition is visible at the trachea inlet for the airways after prosthesis insertion. This is mainly caused by turbulent fluctuations and high tracheal curvature (see Figs. 7e–7h) respect to the healthy geometry. The blockage effect of the prosthesis promotes a considerable redistribution of the locations where the particles deposit. Significant particle concentrations can be found in the region around the prostheses, especially its extremities, as shown in the Figs. 7e–7h) respect to Figs. 7a–7d. The latter drastically increase for increasing particle diameter. In general, for both models it can be seen that an increase of the particle size promotes an increase of deposition for both healthy and stented models and that the increase is more marked for the stented geometries.

The Fig. 8 shows that independently of the flow rate, a marked increase of deposition is promoted by the stented respect to the unstented geometry. Furthermore, in the regions near the stent is visible a progressive increase of deposition (compare Figs. 8a–8c). The superior extremity of the device, that is orthogonal to the stent axis, is affected by an important deposition as seen also before for increasing particle diameter at a fixed flow rate. This location has been found to promote mucous plugging, obstruction and tissue irritation8 so that the presence of drug overdoses may enhance or add negative effect of the presence of the stent. Additionally, a massive increase of deposition is also depicted at the first bifurcation and in the second generation for the stented model. The proximal region of the trachea in the presence of the stent is subjected by a high deposition. This is caused firstly by the airflow that enters skewed the trachea but also by the presence of the device and the promoted blockage effect.

Discussion

The goal of this work is oriented to the investigation of the particle transport and deposition in healthy and stented airways for different flow rates and particle sizes. Special attention has been given to patients that underwent

prosthesis implantation because of the related lack of knowledge. It is known that these devices are prone to obstruct and promote inflammations and other tissue reactions among others negative effects.8,7 Therefore, it is clear that local concentration of toxic particles inhaled in the environment or overdoses of aerosol or other drugs may enhance the aforementioned side effects and further knowledge is necessary for improving eventual therapies and the overall clinical outcomes. In this sense, the prediction of particle deposition in the stented airways regions may be necessary for improving the way of life of the patients. The present work provides a first analysis of particle deposition and transport in stented airways. However, the understanding of the particle deposition within the airways after prosthesis implantation may have different applications as, for example, the improvement of aerosol drug delivery therapies and it may also help reducing in the future the re-interventions after prosthesis placing as well as limiting the number of prosthesis side effects. As an example, a successful drug-aerosol delivery should provide maximum deposition of suitable therapeutic particles in specific sites of interest, which are related to the disease. Also, in the aerosol therapies, the potential negative effects in case of drug overdoses should be minimized.14 The presented results show a local drastic increase of the particle deposition in the stented trachea. The deposition increases in fact in this region respect to the healthy case, as demonstrated by the Weibel-based models. Additionally, the stented regions of the airways, i.e. the first generation and the carina, are also affected by an increased deposition. The findings highlight a particular impact of the Y stent among the considered devices and the trachea seems the place where the highest total deposition occurs. At the same time, in the CT-models, the tracheal stent promotes a massive increase of deposition. These results are especially relevant thinking that they are independent of the breathing conditions and of the particle size. The diameter reduction imposed by the devices promotes a block effect similar to an obstruction.2,30 The deposition of micro particle occurs in fact mainly by impaction, and this includes primary and especially secondary airflow structures that convect inhaled particles to the airway walls.14 The latter may have a negative impact on the tissue reaction that is one of the main problem of a silicone stent. In particular, also independently on the particle size, the presented results show that a considerable increase of deposition is promoted by the presence of the prostheses respect to the healthy airways. Moreover, this result is independent on the particle diameter, as also for small particles the prosthesis tends to allow higher depositions for the aforementioned reasons. As conclusion, these patients are inherently prone to particle deposition in the stented regions and this particle may have different nature such as those coming

from aerosol therapies or those inhaled during the day life. These could be micro or nanoparticles . However, the nanoparticles may not deposit in the first generations,14 where the prosthesis is normally located. Thus, the analysis has been conducted on micro particles that due to their bigger dimensions tend to deposit also in the first generations. An increase of the distribution of deposited particles for these patients may contribute to the development of a different toxicity effect in the regions near the device where the deposition can concentrate and hence interact with the tissues. The latter may finally result in absorption and transport of toxic substances into the tissue, blood and the whole body yet enhancing the possibility of inflammation and further obstructions near the prosthesis and even other disorders.11

The limitations of this work regard the consideration of a limited number of bifurcations, the placement of the bronchial and Ystent only in the healthy Weibel models, the truncation of the model after the larynx and the absence of a direct validation with experiments among others. Additionally, the presented simulations are limited to the assumption of steady state flow conditions thus neglecting any transient effects. For this reason, even the proposed analysis may help improving clinical drug-aerosol targeting and understanding deposition of micro particles for patients that need surgical insertion of an airway prosthesis, the results that can be extrapolated must be taken with careful and they can be used mainly as indication for further experimental and numerical studies.

Acknowledgments

The authors gratefully acknowledge the support of the Spanish Ministry of Industry and Competitiveness through the research Project DPI2017-83259-R (AEI/FEDER,UE). The support of the Instituto de Salud Carlos III (ISCIII) through the CIBER-BBN initiative is highly appreciated.

References

1. Atsou, K., C. Chouaid, G. Hejblum. Variability of the chronic obstructive pulmonary disease key epidemiological data in europe: systematic review. *BMC Med.* 9:7, 2011.

2. Chen, X., W. Zhong, B. Sun, B. Jin, X. Zhou. Study on gas/solid flow in an obstructed pulmonary airway with transient flow based on CFD-DPM approach. *Powder Technol.* 217:252–260, 2012.

3. Chen, X., W. Zhong, X. Zhou, B. Jin, B. Sun. CFD-DPM simulation of particle transport and deposition in pulmonary airway. *Powder Technol.* 228:309–318, 2012.

4. Chen, X., Y. Feng, W. Zhong, B. Sun, F. Tao. Numerical investigation of particle deposition in a triple bifurcation airway due to gravitational sedimentation and inertial impaction. *Powder Technol.* 323:284–293, 2018.

5. Deng, Q., C. Ou, J. Chen, Y. Xiang. Particle deposition in tracheobronchial airways of an infant, child and adult. *Sci. Total Environ.* 612:339–346, 2018.

6. Deng, Q., C. Ou, Y. M. Shen, Y. Xiang, Y. Miao, Y. Li. Health effects of physical activity as predicted by particle deposition in the human respiratory tract. *Sci. Total Environ.* 657:819–826, 2019.

7. Dumon, F. A dedicated tracheobronchial stent. *Chest* 97:328–332, 1990.

8. Dumon, F., S. Cavaliere, J. P. Diaz-Jimenez, J. M. Vergnon, F. Venuta, M. C. Dumon, K. L. Kovitz. Seven-years experience with the dumon prosthesis. J. Bronchol. 3:6–10, 1996.

9. Farkas, A., I. Balásházy. Simulation of the effect of local obstructions and blockage on airflow and aerosol deposition in central human airways. J. Aerosol Sci. 38:865–884, 2007.

10. Farkhadnia, F., T. B. Gorji, M. Gorji-Bandpy. Airflow, transport and regional deposition of aerosol particles during chronic bronchitis of human central airways. *Austral. Phys. Eng. Sci. Med.* 39:43–58, 2016.

11. Hoet, P., I. Brueske-Hohlfeld, O. Salata. Nanoparticles-known and unknown health risks. *J. Nanobiotechnol.* 2:12, 2004.

12. Kadota, K., A. Imanaka, M. Shimazaki, T. Takemiya, K. Kubo, H. Uchiyama, Y. Tozuka. Effects of inhalation procedure on particle

behavior and deposition in the airways analyzed by numerical simulation. *J. Taiwan Inst. Chem. Eng.* 90:44–50, 2018.

13. Kleinstreuer, C., Z. Zhang. Airflow and particle transport in the human respiratory system. *Annu. Rev. Fluid Mech.* 42:301–334, 2010.

14. Kleinstreue, C.r, Z. Zhang, Z. Li. Modeling airflow and particle transport/deposition in pulmonary airways. *Respir. Physiol. Neurobiol.* 163:128–138, 2008.

15. Longest, P. W., M. Hindle, S. D. Choudhuri, J. Xi. Comparison of ambient and spray aerosol deposition in a standard induction port and more realistic mouth-throat geometry. *J. Aerosol Sci.* 39:572–591, 2008.

16. Longest, P. W., S. Vinchurkar, T. Martonen. Transport and deposition of respiratory aerosols in models of childhood asthma. *Aerosol Sci.* 37:1234–1257, 2006.

17. Malvè, M., S. Chandra, J. L. López-Villalobos, E. A. Finol, A. Ginel, M. Doblaré. CFD analysis of the human airways under impedance-based boundary conditions: application to healthy, diseased and stented trachea. *Comput. Biomech. Biomed. Eng.* 16:198–216, 2013.

18. Martonen, T. B., C. J. Musante, R. A. Segal, J. D. Schroeter, D. Hwang, M. A. Dolovich, R. Burton, M. Spencer, J. S. Fleming. Lung models: Strengths and Limitations, Proceedings of the Consensus Conference on Aerosols and Delivery Devices, Bermuda, 1999. *Respir. Care* 45:712–736, 2000.

19. Nowak, N., P. P. Kakade, A. V. Annapragada. Computational fluid dynamics simulation of airflow and aerosol deposition in human lungs. *Ann. Biomed. Eng.* 31:374–390, 2003.

20. Piemjaiswang, R., S. Shiratori, T. Chaiwatanarat, P. Piumsomboon, B. Chalermsinsuwan. Computational fluid dynamics simulation of full breathing cycle for aerosol deposition in trachea: effect of breathing frequency. *J. Taiwan Inst. Chem. Eng.* 97:66–79, 2019.

21. Pourmehran, O., T. Gorji, M. Gorji-Bandpy. Magnetic drug targeting

through a realistic model of human tracheobronchial airways using computational fluid and particle dynamics. *Biomech. Modell. Mechanobiol.* 15:1355–1374, 2016.

22. Pourmhran, O., M. Rahimi-Gorji, M. Gorji-Bandpy, T. Gorji. Simulation of magnetic drug targeting through tracheobronchial airway in presence of an external non-uniform magnetic field using lagrangian magnetic particle tracking. *J. Magn. Magn. Mater.* 393:380–393, 2015.

23. Rahimi-Gorji, M., T. B. Gorji, M. Gorji-Bandpy. Details of regional particle deposition and airflow structures in a realistic model of human tracheobronchial airways: two-phase flow simulation. *Comput. Biol. Med.* 74:1–17, 2016.

24. Rahimi-Gorji, M., O. Pourmehran, M. Gorji-Bandpy, T. Gorji. CFD simulation of airflow behavior and particle transport and deposition in different breathing conditions through the realistic model of human airways. *J. Mol. Liq*. 209:121–133, 2017.

25. Robinson, S. K. Coherent motions in the turbulent boundary layer. *Annu. Rev. Fluid Mech.* 23:601–639, 1991.

26. Van Rhein, T., M. Alzahrany, A. Banerjee, G. Salzman. Fluid flow and particle transport in mechanically ventilated airways. Part I. fluid flow structures. *Med. Biol. Eng. Comput*. 54:1085–1096, 2015.

27. Weibel, E. R. Morphometry of the Human Lung. Springer, New York, 1963.

28. Zhang, Z., C. Kleinstreuer. Airflow structures and nano-particle deposition in a human upper airway model. *J. Comput. Phys.* 198:178–210, 2014.

29. Zhang, Z., C. Kleinstreuer, J. F. Donohue, C. S. Kim. Comparison of micro- and nano-size particle depositions in a human upper airway model. *J. Aerosol Sci.* 36:211–233, 2005.

30. Zhang, Z., S. Qi, Y. Yue, J. Shen, C. Li, W. Qian, J. Wu. Particle disposition in the realistic airway tree models of subjects with tracheal

bronchus and COPD. BioMed Res. Int. 2018:7428609, 2018.